Proceedings of NAPC-2022
National Aerospace Propulsion Conference
19-20 December 2022, IIT Bombay, Powai, Mumbai

NAPC2022-####

NUMERICAL INVESTIGATION & EXPERIMENTAL VERIFICATION OF CENTRALLY LOCATED STRAIGHT STRUT INJECTOR FOR SCRAMJET COMBUSTOR: STUDY ON EFFECT OF STEP-LIKE MODIFICATIONS ON MIXING CHARACTERISTICS

Joseph Noel Kiren[1], Abraham Kevin Clifford[1],
Akash Raja Anbarasu[1], Gulam Rabbani Ebne Sattar[1], G. Dinesh Kumar[2]

[1]Student, Bachelor of Aeronautical Engineering, Hindustan Institute of Technology and Science, Chennai
[2]Assistant Professor, Department of Aeronautical Engineering, Hindustan Institute of Technology and Science, Chennai

ABSTRACT

Centrally located wedge-strut injector is a common type of scramjet injector tried and tested and in use for considerable time, this study focusses on the computational analysis and experimental verification of the wedge strut geometry with step-like modifications at the trailing edge and study the effect it has on the combustion performance. Numerical evaluation is carried out for the straight strut geometries which is placed inside a test section with the inlet flow speed fixed at Mach 2, and inlet jet diameter fixed at 0.6mm, the fuel (hydrogen) is injected at a speed of Mach 2.3. After a solution is reached, the density contour is acquired and a brief observation of the various flow phenomenon (oblique shocks, expansion waves & shock diamonds) and the interactions (shock-shock & shock-boundary layer) and their contributions towards increasing mixing efficiency by the inducing of turbulence and vorticity is discussed. To determine the enhancement of combustion performance we analyze the zone of recirculation, fuel mole fraction, velocity profile and total pressure decay plots at the wake region of the strut. The geometry with single step is selected for experimental verification (coldflow). For the experimental verification, the numerically predicted wall static pressure plots and density contours are compared with the experimentally extracted wall static pressure values and shadowgraph contours respectively and were found to be in good agreement.

Keywords: Straight strut; Hydrogen; Turbulence; Vorticity; Recirculation zone; Total pressure decay

NOMENCLATURE

k	Turbulent kinetic energy
ω	Specific dissipation rate
ν_T	Kinematic eddy viscosity
Pa	Pascal
K	Kelvin
Y_f	Species mass fraction
P	Pressure
u_i, u_j	Velocity
o	(subscript) Stagnation condition
j	(subscript) Jet exit condition

1. INTRODUCTION

A scramjet engine is essentially a ramjet engine adapted for combustion of supersonic airflow. It relies on the high speed of the vehicle to compress the air much like the ramjet engine which however combusts in the subsonic regime using nose inlet cones and a series of shocks to progressively slow down the supersonic flow and finally rendering it subsonic with a weak normal shock and proceeds to combust the subsonic airflow. Whereas the scramjet which lacks any of these, having only a variable area inlet it controls the supersonic speed of the airflow to a certain level and combusts the flow in supersonic regime, this allows it to be used efficiently for high supersonic and hypersonic speed applications especially in the military (mostly in cruise missiles) and space exploration (as launch vehicles). The disadvantage however is that these engines cannot start from rest and have to be accelerated to a sufficient speed to achieve the necessary compression and hence start operating (this is done by means of launch platforms and rocket assist (JATO) etc.) and their low combustion efficiencies and run times. The Scramjet's potential has inspired experts from all around the globe to focus on enhancing the engine's combustion efficiency by improving the mixing and residence time of the air-fuel mixture. Because the flow across the inlet is still supersonic, combustion in the combustion chamber is a difficult task as the residence time of the air-fuel mixture is very short usually in order of milliseconds [12].

Challenges to scramjet combustion operation include lack of good mixing and thrust losses, of which there are a few,

notably because of incomplete mixing, viscous effects and shockwaves. Shockwaves are imminent in any supersonic flow, however we can make use of them to help with the mixing [6], as shockwaves may cause spreading of the shear layer downstream from the point of shock-shear layer interaction [13] and are accompanied by turbulence and vorticity [5], but on the flipside these also contribute to the thrust losses. [6]. Initially, fuel was injected in a transverse fashion, this method causes a significant recirculation region and greatly improves the combustion efficiency, however this type of injection causes a normal shock and hence leads to a significant total pressure loss. Strut based injector mechanism designs were developed to counter this, and have shown good potential, mainly as it enables the fuel to be injected into the core of the flow and hence provides a uniform spread of the fuel. [5].

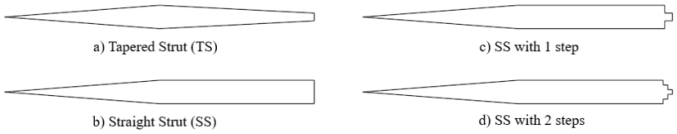

FIGURE 1: SCHEMATICS OF TAPERED STRUT, STRAIGHT STRUT AND STRAIGHT STRUT WITH OUR MODIFICATIONS

For our study we select a wedge type straight strut (SS) based injector, as the straight strut design offers a larger recirculation region than tapered strut (TS). [5]. We also fix the jet inlet diameter to be 0.6mm as it proved more effective for mixing than when compared to larger diameters i.e., 1mm & 2mm [5]. Hydrogen is selected as fuel. Having selected our base design, we apply some modifications to it by introducing step like modifications on the aft section of our geometry. We hypothesize that this would cause turbulence and higher recirculation in the wake region.

Firstly, we replicate the modified geometry of the strut using a designated software and simulate the operational parameters using CFD software. Having zeroed in on the most desirable geometry we carry forward with the experimental evaluation of our CFD results.

2. EXPERIMENTAL AND NUMERICAL METHODOLOGY

2.1 Numerical Method

2.1.1 Turbulence model

The computational study is carried out using ANSYS FLUENT software. In this study a type of Renolds Average Navier Stokes (RANS) turbulence model called the Shear Stress Transport (SST) k-omega is used. The solver used is density based and the flow is set to follow ideal gas law. For simulating combustion, a species transport and eddy-dissipation turbulence chemistry interaction model has been employed.

2.1.2 Governing Equations

Renolds Average Navier Stokes (RANS) is a numerical method which describes a turbulent flow field. It is a reduced form of general Navier Stokes equation. Further modification of it will result in one equation or two equation turbulence models. The SST k-ω is a two equation turbulence model, which is based on the standard k-ε and the standard k-ω model [8]. It combines the characteristics of both of these models where k-ε predicts the flow field outside the boundary layer (core-flow) and k-ω predicts the flow field within the boundary layer (near walls). The governing equations of the turbulence model is as follows:

Mass conservation (Continuity equation)

$$\frac{\partial \rho}{\partial t} + \frac{\partial}{\partial x_i}(\rho u_i) = 0 i = 1,2 \quad (1)$$

Momentum conservation

$$\frac{\partial}{\partial t}(\rho u_i) + \frac{\partial}{\partial x_i}(\rho u_i u_j) = -\frac{\partial P}{\partial x_i} + \frac{\partial}{\partial x_i}(\tau_{ij}) i,j = 1,2 \quad (2)$$

Energy equation

$$\frac{\partial}{\partial t}(\rho e_t) + \frac{\partial}{\partial x_i}(\rho h_t u_i) = \frac{\partial}{\partial x_i}(\tau_{ij} u_i - q_i) i,j = 1,2 \quad (3)$$

SST k-ω governing equations:

Turbulent kinetic energy

$$\frac{\partial k}{\partial t} + U_j \frac{\partial k}{\partial x_j} = P_k - \beta^* k\omega + \frac{\partial}{\partial x_j}\left[(\nu + \sigma_k \nu_T)\frac{\partial k}{\partial x_j}\right] \quad (4)$$

Specific dissipation rate

$$\frac{\partial \omega}{\partial t} + U_j \frac{\partial \omega}{\partial x_j} = \alpha S^2 - \beta \omega^2 + \frac{\partial}{\partial x_j}\left[(\nu + \sigma_\omega \nu_T)\frac{\partial \omega}{\partial x_j}\right] + 2(1 - F_1)\sigma_{\omega 2}\frac{1}{\omega}\frac{\partial k}{\partial x_i}\frac{\partial \omega}{\partial x_i} \quad (5)$$

Where, k is turbulent kinetic energy, ω is specific turbulent dissipation rate, F1 is the blending Function, ν_T is kinematic eddy viscosity, F2 is second blending function, Pk is production limiter, and S is user defined source term.

2.1.3 Grid study

A 2D structured mesh is created where the cells are more refined closer to the wall and surfaces of the strut. For finding a suitable grid size, three different grid sizes of 77,600, 147,300 and 286,000 elements were chosen and the wall static pressure parameter has been used to observe the variation in the results. All the three grids produced close enough results to each other, and we chose a grid that we felt was optimal considering the computational time and cost needed.

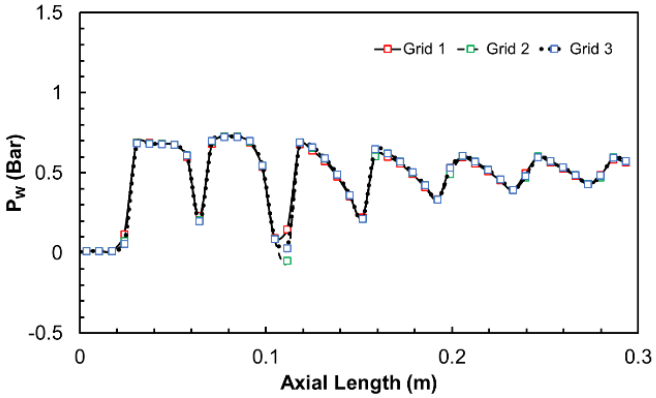

FIGURE 2: GRID INDEPENDENCE STUDY, WALL STATIC PRESSURE COMPARISON

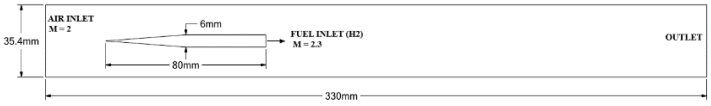

FIGURE 3: SCHEMATIC VIEW OF THE COMPUTATIONAL DOMAIN OF THE RECTANGULAR COMBUSTOR WITH SS

2.1.4 Validation study

Our computational domain [Fig 3] consists of a rectangular combustor of 330mm in length and 35.4mm in height. At 30mm from the inlet, a strut is located centrally. The strut is 80mm long and has a thickness of 6mm. It is tapered from its leading edge till its midpoint, and is straight edge from the midpoint till its trailing edge. Hydrogen fuel is injected from a 0.6mm diameter inlet at the base of the strut.

TABLE 1: FLOW INPUT PARAMETERS

Parameter	*Air*	*Hydrogen*
Mach no.	2	2.3
Pressure, Pa	49.5	29.5
Temperature, K	159	151
Y_{O2}	0.23301	0
Y_{H2}	0	1
Y_{N2}	0.76699	0

For validating our numerical setup, the rectangular combustor dimensions along with the Straight Strut (SS) geometry from [5] is used as the reference and we compare the results of the density gradient contour and mole fraction plot at x = 83mm. The flow input parameters were taken from the reference paper [5] and are tabulated at [Table 1]. The air enters the domain at Mach 2 and the hydrogen fuel enters at Mach 2.3 from the base of the strut. The density gradient contour of the SS from the reference paper and the density contour from our results are compared in [Fig 4]. And the mole fraction graph is compared in [Fig 5].

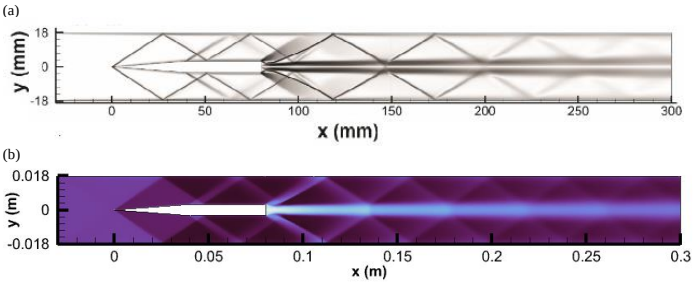

FIGURE 4: (a) DENSITY GRADIENT CONTOUR FROM REF [5] (b) DENSITY CONTOUR FROM OUR ANALYSIS.

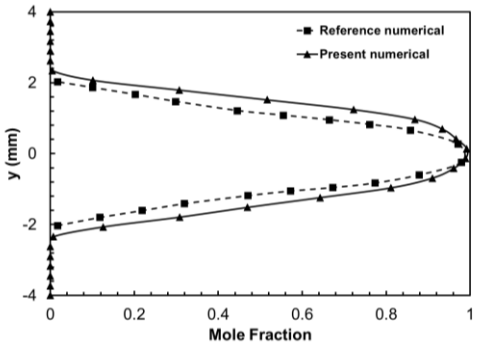

FIGURE 5: MOLE FRACTION COMPARISION PLOT AT X=83MM DISTANCE

2.2 Experimental Method

2.2.1 Experimental setup

Based on the CFD analysis we select the single-step straight strut geometry for experimental evaluation (coldflow). The experiment was conducted in a blow down type wind tunnel setup in a high-speed jet facility. The high-speed jet facility [Fig 6] consists of a condenser to remove the moisture from atmospheric air, this is then fed into two compressor pumps (20hp each) which then charge the high pressure tank (8000L total capacity). Once sufficient pressure is reached the compressors auto cutoff and the pressurized flow is let into the settling chamber by a valve, this is then opened into our CD nozzle, test section duct and the flow turns supersonic at the throat of the CD nozzle.

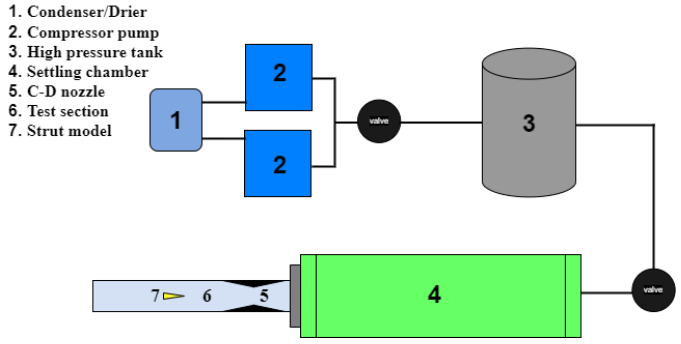

FIGURE 6: SCHEMATIC LAYOUT OF THE HIGH SPEED JET FACILITY

To maintain a flow of Mach 2 the minimum pressure required in the settling chamber is 7.92 bar which is calculated from the isentropic pressure ratio equation.

$$\frac{\mathbf{p}}{\mathbf{p}_t} = \left(\mathbf{1} + \frac{\gamma-1}{2}\mathbf{M}^2\right)^{\frac{-\gamma}{\gamma-1}} \quad (6)$$

2.2.2 Designing the nozzle

For our required flow condition of Mach 2, a suitable CD nozzle is designed with consideration of our test section's dimensional requirements. Our proposed dimension for the test section is 200mm × 36mm. With the area-Mach number relation for isentropic flows [Eq 7], our nozzle throat area is calculated to be at 21.33mm.

$$\frac{A}{A^*} = \left(\frac{\gamma+1}{2}\right)^{-\frac{\gamma+1}{2(\gamma-1)}} \frac{\left(1+\frac{\gamma-1}{2}\mathbf{M}^2\right)^{\frac{\gamma+1}{2(\gamma-1)}}}{\mathbf{M}} \quad (7)$$

There are two kinds of nozzles namely a) Gradually expanding nozzles, and b) Minimum length nozzles. A gradually expanding nozzle has two sections – expansion section and straightening section and it will be longer because of this. It is employed in applications where the importance is at maintaining a high quality flow at the exit. A minimum length nozzle gets rid of the expansion section by doing so reduces the overall length of the nozzle. It is employed for applications where the size and weight are of more importance. Since our application is for a wind tunnel, a gradually expanding nozzle is more suitable. The geometry of the nozzle was designed in a way that it reduces the strength of the expansion waves emerging from the throat and also the oblique shocks from the nozzle-test section interaction. The test section will be an extension from the nozzle's exit. So far, we have used only 2D analysis, we arbitrarily assign the width to be 15mm.

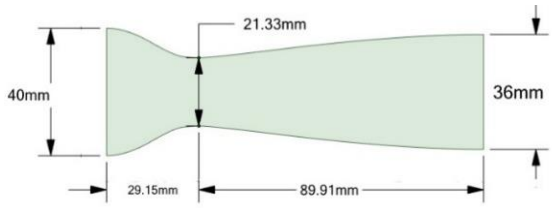

FIGURE 7: CD NOZZLE DESIGNED FOR MACH 2

2.2.3 Design and fabrication of the test assembly

In this phase we plan and design a suitable enclosure consisting of several components that will enclose our control volume. Mild steel is our chosen material for all the metal components. The main tunnel assembly is designed to hold the shape of our control volume [Fig 8] to its designated dimensions. And on the bottom, there are ports for taking pressure readings. Within the tunnel we have our test object which is the strut (placed centrally and wall to wall). On both the sides we have acrylic glass for shadowgraph flow visualization. Finally, a suitable linking mechanism (Disk/Flange) to mate the entire setup to the high speed jet facility is designed. Having built all the individual components, we assemble them to form our complete model [Fig 9]

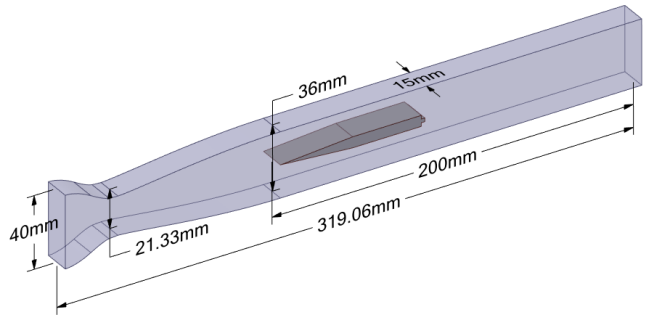

FIGURE 8: PROPOSED CONTROL VOLUME WITH STRUT

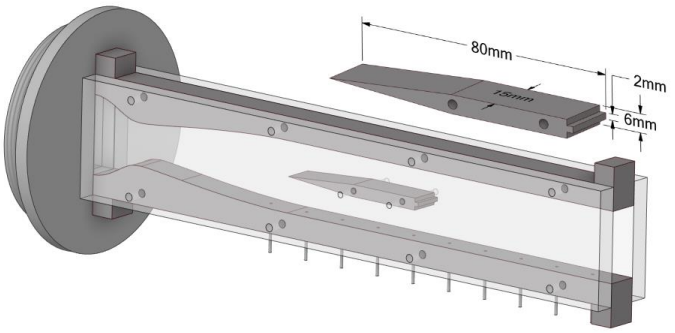

FIGURE 9: FINAL MODEL OF OUR TEST ASSEMBLY

2.2.4 Shadowgraph setup

The shadowgraph setup [Fig 10] consists of a high intensity lamp, which emits high energy light beams, this is made to fall on a convex lens which focusses the beam onto a mirror, the mirror then reflects the beams onto a screen, the model is placed in between the mirror and screen [Fig 11], a high speed camera is kept focused on the shadow on the screen. Once the supersonic stream flows into the test section shocks are developed, the shadows of these shocks are seen on the screen (as they refract light rays) and are recorded by the camera, the image is then extracted from the video and enhanced.

FIGURE 10: VISUALIZATION ARRANGEMENT: 1. LIGHT SOURCE, 2. LENS, 3. MIRROR, 4. CAMERA.

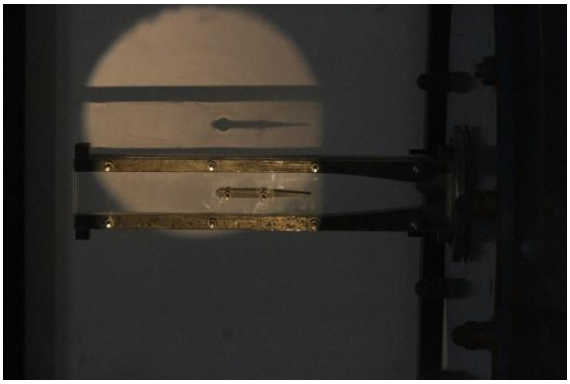

FIGURE 11: VISUALIZATION THROUGH SHADOWGRAPH

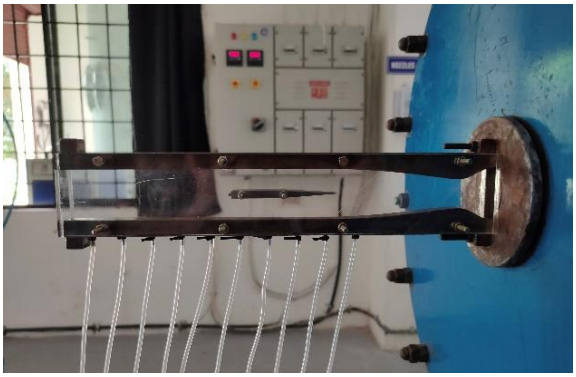

FIGURE 12: MODEL FITTED WITH SILICONE TUBES FOR STATIC PRESSURE MEASUREMENT

Silicone tubes are attached to the pressure ports [Fig 12] and fed into the pressure scanner (16 port electronic pressure scanner) and the test run is carried out, the recorded data is in form of signal files and it is decoded and read by the designated software. The port wise average of these pressure values recorded at progressive time instances is plotted against the axial length. This graph is used for evaluative studies.

3. RESULTS AND DISCUSSION

3.1 Flow features

Based on the computational analysis of the base and the modified geometries and the comparison of contours and graphical plots plotted thereof, we can state that though there are marginal jumps in static pressure [Fig 13] we don't have any significant changes between the base and modified strut geometries. However, for further experimental evaluation we select the single strut geometry.

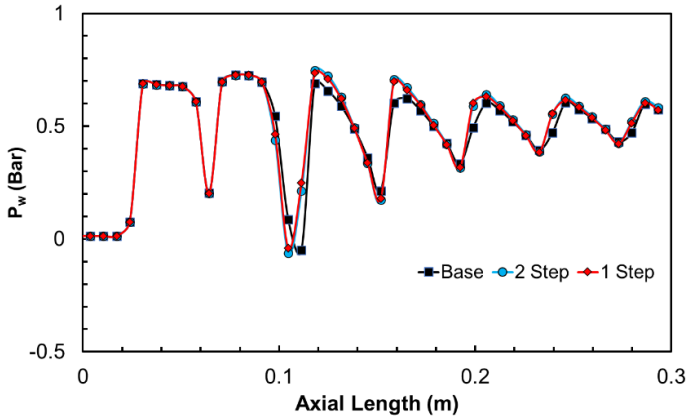

FIGURE 13: WALL STATIC PRESSURE COMPARISION

As the supersonic flow encounters the strut [Fig 14] an oblique (compression wave) shock attaches to the leading edge of the strut and it is reflected off the walls, as the taper ends at 40 mm from the leading edge, the flow is turned away from itself causing a slight acceleration which hence results in an expansion wave, the oblique shock then reflects off the wall and strut causing a shock diamond. At the end of the strut the flow is yet again turned away from itself and there is a sudden increase of flow area downstream, this causes a sudden acceleration of the flow and an expansion wave much powerful than the first is generated. The oblique shock is then reflected back and forth between the upper and lower walls forming a shock train for the remaining length of the test section.

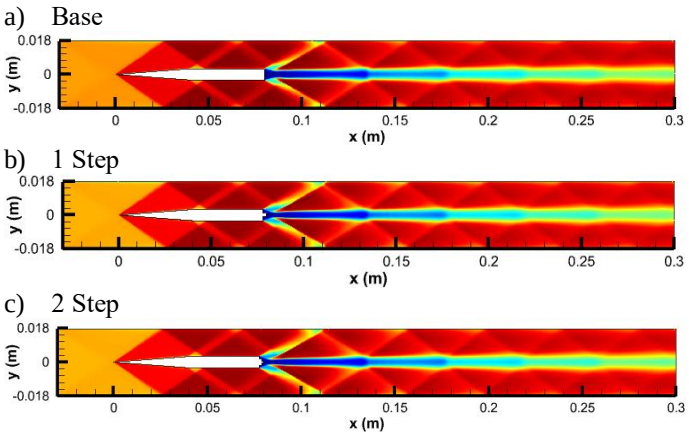

FIGURE 14: DENSITY CONTOUR COMPARISON

From the density contours it is observed that at the shock-shear interaction point the fuel jet is broken up and this enhances the mixing. The instability thus caused also enhances vorticity. [5]. It was also observed [2] shock strength encourages vorticity production. Also noticeable is the shock-boundary layer interaction at the test section walls, this causes boundary layer separation which leads to vortice shedding downstream of the injection, this has a positive effect on the mixing. Jumps in vorticity corresponds directly to the shock wave and shock diamonds, this implies that compressibility directly influences vorticity which in turn enhances better mixing [3]. However presently the shock boundary layer interaction contributes a very negligible effect for our case.

At the aft section of the strut geometry a recirculation region [Fig 15] is visible, the intensity of the recirculation influences the air-fuel mixing and the bigger the zone of recirculation the larger the turbulence generated. The intensity of the recirculation induced at the aft section of the geometry influences the fuel jet dispersion and mixing of the dispersed fuel with the air.

From figure 15, it is evident that the recirculation regions are comparable between the three cases. It can also be noticed that the presence of steps causes the recirculation region to adhere to the step corner, i.e., Closer to the strut wall.

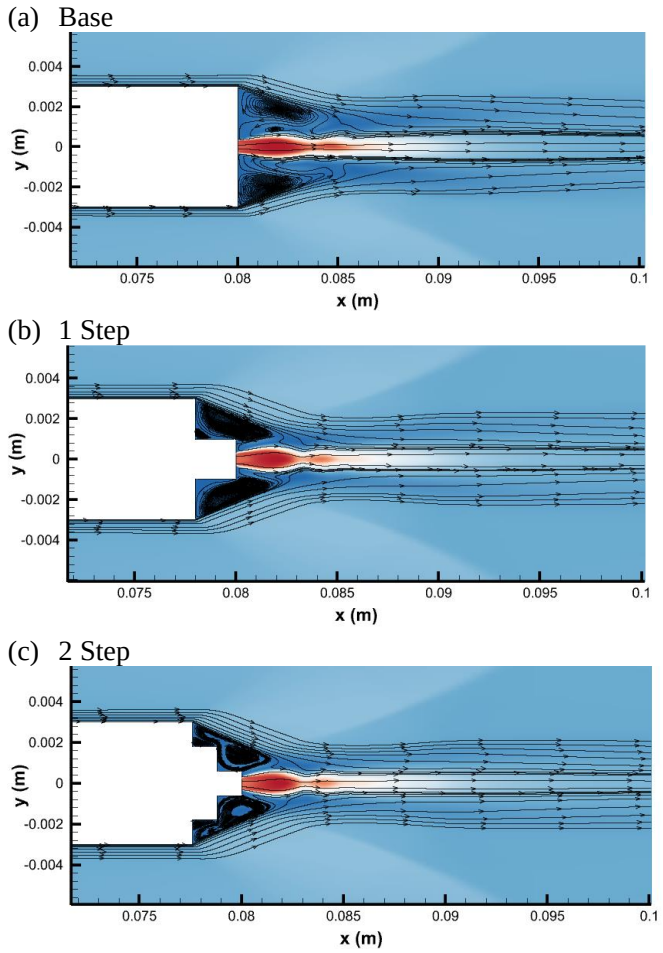

FIGURE 15: RECIRCULATION REGION AT THE BASE OF THE STRUT

Figure 16 compares the mole fraction plot at different locations. It can be noted that at 83mm [Fig 16(a)] which is near the point of injection, the fuel dissipates a little faster for the unstepped case (Base), this can be said due to its larger area overlapping the curves for both step 1 and 2. However we notice that at 130mm [Fig 16(b)] the stepped struts fair marginally better in the central core shear flow region than the unstepped strut as the curves of both single and double step are similar and have a marginally larger area than the unstepped strut, indicating a larger dissipation among stepped geometries especially close the fuel jet induced shear layer, as the larger area corresponds towards the peak of the curve i.e. central region, the unstepped strut however reached a marginally better dissipation away from the center and towards the walls. We notice that at 180mm [Fig 16(c)] there is no difference in dissipation between the stepped and unstepped regions, as the three curves are near identical.

From the above stated information, we can see that the dissipation occurs principally in the direction along the flow i.e., streamwise direction. One of the reasons for poor fuel dissipation in the transverse (region perpendicular to the direction of the flow) direction is the small velocity gradient between the oncoming airstream flow and the injected fuel jet flow.

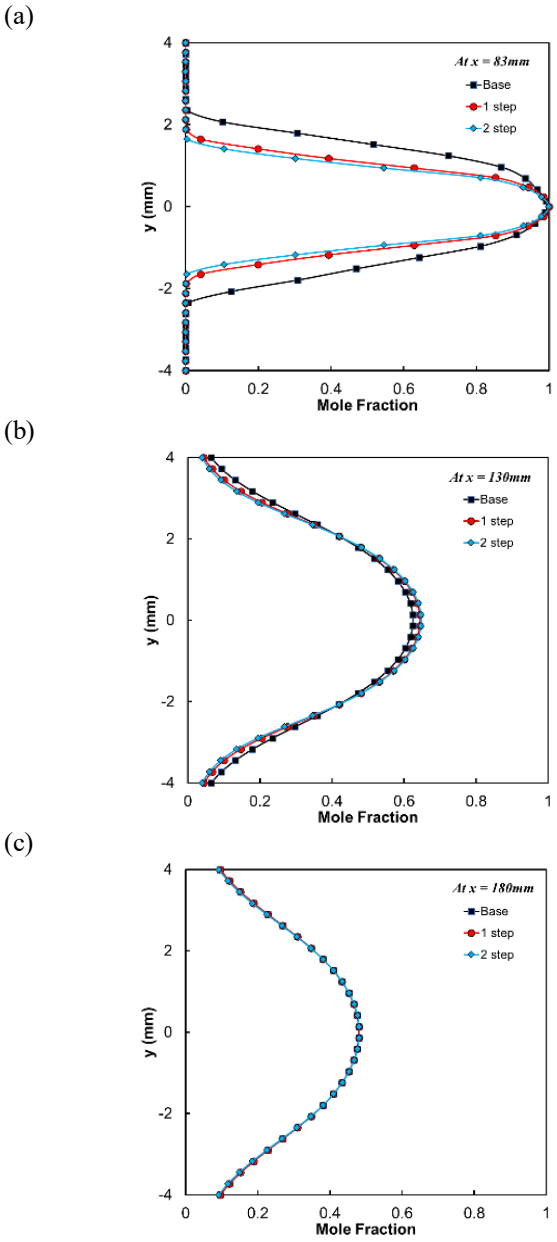

FIGURE 16: MOLE FRACTION AT DIFFERENT LOCATIONS

In Figure 17 the normalized velocity plots for downstream locations helps us determine the increment of fuel jet dissipation and mixing. At 83mm [Fig 17(a)] we can notice that for all cases, the velocity is maximum at the centerline where the fuel jet induced shear stream is located (between +1mm and -1mm). Also apparent is the dip in velocity at the recirculation regions just above and below the point of injection (between 0 and ±1), this establishes that a recirculation region corresponds to a reduced velocity as when compared to the velocity of the ambient flows, i.e. Normalized velocity, it can be noticed that the peak velocity for the stepped struts are lower than that for unstepped strut, also it can be noticed that the single step strut geometry reaches a lower velocity at the recirculation region

than other cases, a lower velocity directly corresponds to a higher residence time for the fuel which enhances the mixing, the double step strut has a similar velocity profile to that of the single step strut, however for the unstepped strut the velocity seems to dip sooner, indicating a wider wake region behind the unstepped strut.

At 130mm [Fig 17(b)], the normalized jet velocity plots shows considerable deceleration of over 70% as when compared to 83mm location, here the stepped struts have comparable profiles and the unstepped strut has a marginally lower velocity, these differences are however nullified at 180mm [Fig 17(c)] where the profiles of all cases are near identical and face a velocity reduction of over 80% as when compared to the 83mm location.

(a)

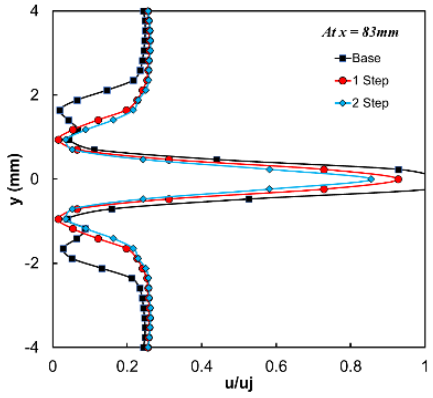

(b)

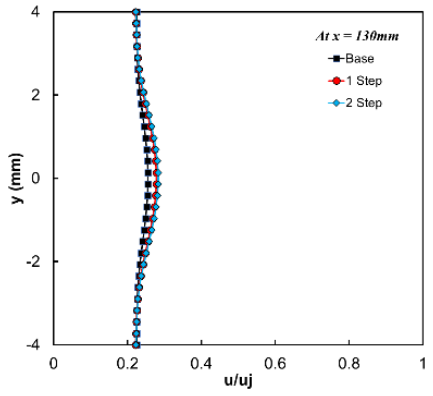

(c)

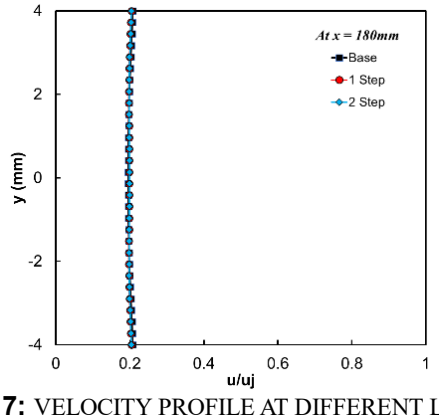

FIGURE 17: VELOCITY PROFILE AT DIFFERENT LOCATIONS

3.2 Total pressure decay

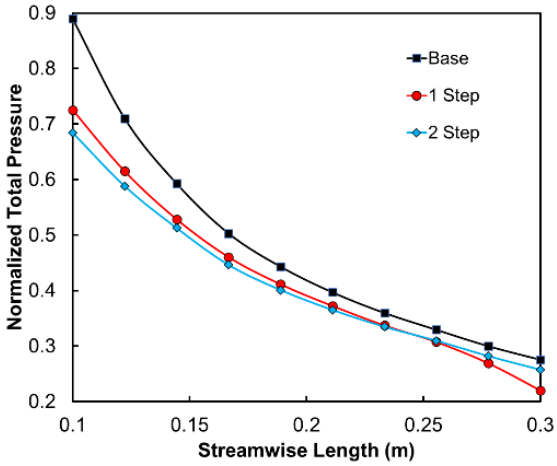

FIGURE 18: TOTAL PRESSURE DECAY COMPARISION

For evaluation of supersonic injection mixing and combustion we make use of total pressure and temperature decay plots [4] to analyze. For our case owing to the minute change in temperature parameters provided by our main source paper [5] total temperature decay cannot be used to effectively analyze the cases, so total pressure decay is selected for analysis and the graph for all three cases are plotted and compared. Figure 18 shows the total pressure decay plot for points taken along the centerline, inside the fuel jet induced shear flow, and the stagnation pressure is normalized using the formula stated: $(P_o - P_{oj}) / P_{oj}$.

Total pressure decay is an effective method to study the fuel dissipation and mixing, a faster decay of total pressure indicates a higher degree of dissipation pointing to an improvement in mixing.

From the total pressure decay, it can be seen that the starting total pressures of stepped struts are lower than unstepped strut and also reaches a lower stagnation pressure, single step strut reaching the lowest, the rate of decay is almost comparable, being steep upto 0.2m and the slope flattens from there. The stagnation pressure for single strut decays again starting at 0.25m and the curve steepens considerably again for the said case. Considering the above computational analysis, the single step strut geometry is selected for further experimental analysis.

3.3 Comparison with experimental data

Since our experiment has been conducted for a coldflow, and in order to compare the results, a numerical coldflow CFD simulation with the exact dimensions of the entire duct along with the C-D nozzle has also been done. The shadowgraph image of the test section of the experiment is found to be in good agreement with the numerical method developed contour for density. See Figure 19.

The static pressure readings obtained from the pressure ports by the pressure scanner, the information is stored in form of signals and is read by using a suitable software, the values

which were recorded for a set time in 0.5 second intervals are sampled, and the averaged values are obtained, the values thus obtained are in imperial units- pound per square inch (psi), they are converted into newton per square meter (pascals) and are plotted with respect to the corresponding locations of these ports along the axial length and a curve is generated for the experimental data. For the numerical data, rake points are placed at the exact locations of the pressure ports and static pressure readings for the said conditions are extracted after numerical computation, these values are plotted similar to experimental plot, and the curve is developed for numerical analysis. In Figure 20 the plots of numerical and experimental data are compared and are found to be in good agreement.

(a)

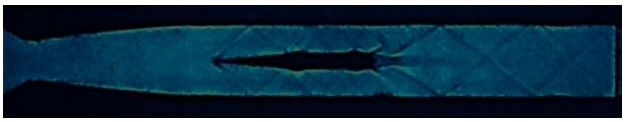

(b)

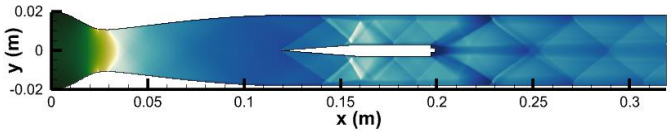

FIGURE 19: (a) EXPERIMENTAL SHADOWGRAPH IMAGE COMPARED WITH (b) NUMERICAL DENSITY CONTOUR

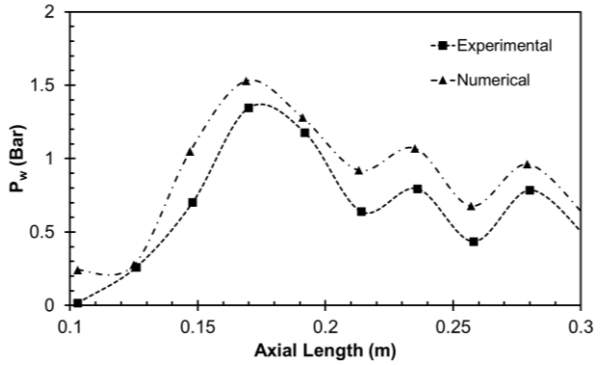

FIGURE 20: WALL STATIC PRESSURE COMPARISON

The pattern of these curves is comparable. However, owing to various losses the curve contour for experimental data is lower than the curve contour for numerical data. Initially the pressure increases steadily as the supersonic flow encounters the strut and oblique shock is generated and attaches to the leading edge of the strut. The first peak occurring at about 0.17m corresponds to the increase in pressure due to the oblique shock hitting the wall near here, the pressure drops again as the flow continues to accelerate a little and is slowed down yet again by an oblique shock wave of a lower strength, and a smaller pressure peak is achieved at about 0.24m. This trend continues for one more peak before the end of the test section is reached.

4. CONCLUSION

The numerical evaluation carried out for the straight strut geometries yielded vital data with respect to the air-fuel mixing, which is most important for an improved combustion performance. The merits of including step like modifications at the trailing edge of the strut are small. There is indeed an improvement (albeit a small one) in fuel dissipation as concluded from the total pressure decay graph. From this study it can be concluded that for the given operational parameters, inclusion of step like modifications to the straight strut trailing edge does not significantly improve the combustion performance in the scramjet combustor.

ACKNOWLEDGEMENTS

We would like to thank: The Aeronautical department of KCG Institute of Technology and Science, Karapakkam, Chennai; for permitting us to use their high speed jet facility. Mr. Dinesh Kumar (asst. prof, HITS) for being our research guide. Mr. Venkat Ramanan (asst. prof, KCG) for making our experimental analysis possible. Mr. Raadha Krishnan (student, HITS) for helping us carry out testing and data gathering from our model. Mr. Akash Raja (student, HITS) and Mr. Rabbani (student, HITS) for helping us with model fabrication.

REFERENCES

[1] Seshadri, P. K., & De, A. (2020). Investigation of shock wave interactions involving stationary and moving wedges. Physics of Fluids, 32(9), 096110.

[2] Ben-Dor, G., Dewey, J. M., & Takayama, K. (1987). The reflection of a plane shock wave over a double wedge. Journal of Fluid Mechanics, 176, 483-520.

[3] Cecere, D., Ingenito, A., Romagnosi, L., Bruno, C., & Giacomazzi, E. (2010, July). Shock/boundary layer/heat release interaction in the HyShot II Scramjet combustor. In 46th AIAA/ASME/SAE/ASEE Joint Propulsion Conference & Exhibit (p. 7066).

[4] Charyulu, B. V. N., Kurian, J., Venugopalan, P., & Sriramulu, V. (1998). Experimental study on mixing enhancement in two dimensional supersonic flow. Experiments in fluids, 24(4), 340-346.

[5] Soni, R. K., & De, A. (2017). Investigation of strut-ramp injector in a Scramjet combustor: Effect of strut geometry, fuel and jet diameter on mixing characteristics. *Journal of Mechanical Science and Technology*, *31*(3), 1169-1179.

[6] Gerlinger, P., & Bruggemann, D. (2000). Numerical investigation of hydrogen strut injections into supersonic airflows. Journal of Propulsion and Power, 16(1), 22-28.

[7] Pandey, K. M., & Sivasakthivel, T. (2011). CFD analysis of mixing and combustion of a scramjet combustor with a planer strut injector. International Journal of Environmental Science and Development, 2(2), 102.

[8] Choubey, G., & Pandey, K. M. (2017). Numerical studies on the performance of scramjet combustor with alternating wedge-shaped strut injector. International Journal of Turbo & Jet-Engines, 34(1), 11-22.

[9] Athithan, A. A., Jeyakumar, S., Sczygiol, N., Urbanski, M., & Hariharasudan, A. (2021). The Combustion Characteristics of Double Ramps in a Strut Based Scramjet Combustor. Energies 2021, 14, 831.
[10] Bao, W., Zong, Y., Chang, J., & Cui, T. (2012). Effects of strut swept angle on the drag of scramjet. Proceedings of the Institution of Mechanical Engineers, Part G: Journal of Aerospace Engineering, 226(4), 455-466
[11] Suneetha, L., Randive, P., & Pandey, K. M. (2019). Numerical investigation on influence of diamond shaped strut on the performance of a scramjet combustor. International Journal of Hydrogen Energy, 44(13), 6949-6964.
[12] Relangi, N., Ingenito, A., & Jeyakumar, S. (2021). The implication of injection locations in an axisymmetric cavity-based scramjet combustor. Energies, 14(9), 2626.
[13] Menon, S. (1989, January). Shock-wave-induced mixing enhancement in scramjet combustors. In 27th Aerospace Sciences Meeting (p. 104).